Hydrophobic Core around Tyrosine for Human Endothelin-1 Investigated by Photochemically Induced Dynamic Nuclear Polarization Nuclear Magnetic Resonance and Matrix-Assisted Laser Desorption Ionization Time-of-Flight Mass Spectrometry

Hiroyuki Takashima,*[,‡] Haruhiko Tamaoki,[§] Naoki Teno,[‡] Yoshinori Nishi,[||] Susumu Uchiyama,[⊥] Kiichi Fukui,[⊥] and Yuji Kobayashi[||]

Novartis Institutes for BioMedical Research, Novartis, Ohkubo 8, Tsukuba, Ibaraki 300-2611, Japan, Graduate School of Medical Sciences, University of Kumamoto, 1-1-1, Honjo, Kumamoto 860-8556, Japan, Graduate School of Engineering, Osaka University, 1-6 Yamadaoka, Suita, Osaka 565-0871, Japan, and Graduate School of Pharmaceutical Sciences, Osaka University, 1-6 Yamadaoka, Suita, Osaka 565-0871, Japan

Received June 29, 2004; Revised Manuscript Received August 6, 2004

ABSTRACT: Human endothelin-1 (ET-1) is a potent cardiovascular bioactive peptide. Its activity is based on the C-terminal residues, e.g., Trp 21 in particular. Recently, we reported an NMR solution structure of ET-1, which has a C-terminal hydrophobic core around Tyr 13. This C-terminal conformation does not agree with a previously reported X-ray crystal structure. To clarify the discrepancy, we performed photo-CIDNP NMR in combination with MALDI-TOF MS. The photo-CIDNP results revealed that the Tyr 13 aromatic ring is concealed in a hydrophobic interaction. MALDI-TOF MS experiments showed this is an intramolecular interaction in monomeric form, which is also supported by sedimentation analysis and two-dimensional NMR cross-peak line shapes. Thus, we confirmed the intramolecular hydrophobic core around Tyr 13 in aqueous solution, which agrees with the solution structure. The C-terminal conformational discrepancy between the solution and crystal was caused by the intermolecular hydrogen bond between Tyr 13 of one molecule and Asp 8 of the other in a dimer-like formation of crystalline ET-1. On the other hand, we indicated that endothelin-3, another isoform of the endothelin, has an apparent self-association equilibrium under the same condition in which three tyrosines participate.

Human endothelin-1 (ET-1)[1] is a potent cardiovascular bioactive peptide (*1*). Because of its complex bioactivities related to heart failure, hypertension, angiogenesis, cancer, etc. (*2*−*5*), ET-1 has been an important target for drug discovery at many pharmaceutical companies. The three-dimensional structures of ET-1 have been determined by X-ray crystallography and NMR spectroscopy (*6*−*10*); however, there was a large conformational discrepancy in the C-terminal part, which is conserved in the endothelin family and is unambiguously critical for the bioactivities (*11*). The discrepancy mainly resulted from structural dispersion of the part in the solution structures (*7*−*10*). Therefore, for years, only an ET-1 crystal structure (*6*) has been utilized in the drug design process for the ET-1 receptor antagonists. The most important pharmacophore of ET-1 is a residue, Trp 21, which is located apart from the other aromatic residues, such as Tyr 13 and Phe 14, in the crystal structure. However, all of the ET-1 receptor antagonists developed previously have close assembling of their aromatic rings (*12*, *13*). Does the ET-1 crystal structure really represent the active conformation as expected? Our results reported here provide the answer.

Very recently, we reported a refined solution structure of ET-1 (*14*) using a new procedure for the NMR data-based molecular dynamics calculations, and deposited the structure in the Protein Data Bank as entry 1v6r. This procedure uses a distributed computing technique (*15*) to increase the number of initial structures, up to tens of thousands, to increase conformational sampling. Like the previous NMR and X-ray structures (*6*−*10*), the refined structure has an α-helix and extended β-strand, which are stabilized by two disulfide bonds in the N-terminus. The unique folding, termed a cystine-stabilized α-helix motif (CSH motif), was originally discovered in ET-1 (*7*) and was investigated for a series of peptides in various species (*16*−*20*). Because of the CSH motif, the previous studies were in agreement about the N-terminal structure. However, because of this, they have dispersed C-terminal structures (*14*).

The refined structure (*14*) has a well-defined folding in the C-terminal part, as well as the CSH motif region. The C-terminal part has an extended β-structure and is loosely looped back to the α-helix by a turn in the junction, forming

* To whom correspondence should be addressed: Informatics and Knowledge Management at Novartis Institutes for BioMedical Research, Novartis Pharma, Ohkubo 8, Tsukuba, Ibaraki 300-2611, Japan. Phone: +81-29-865-2285. Fax: +81-29-865-2385. E-mail: hiroyuki.takashima@novartis.com.

‡ Novartis.

§ University of Kumamoto.

|| Graduate School of Pharmaceutical Sciences, Osaka University.

⊥ Graduate School of Engineering, Osaka University.

[1] Abbreviations: CSH motif, cystine-stabilized α-helix motif; ET, human endothelin; MALDI-TOF MS, matrix-assisted laser desorption ionization time-of-flight mass spectrometry; NMR, nuclear magnetic resonance; photo-CIDNP, photochemically induced dynamic nuclear polarization.

10.1021/bi048649u CCC: $27.50
Published on Web 10/16/2004

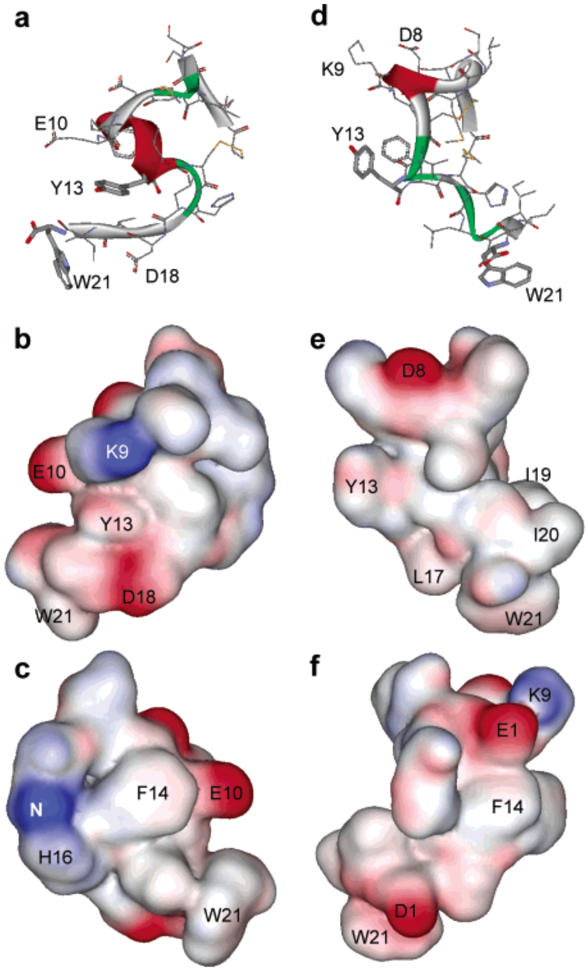

FIGURE 1: Structural comparison of solution and crystalline ET-1 and the hydrophobic core around Tyr 13 in solution. (a) Minimum energy structure in solution with the α-carbon ribbon (PDB entry 1V6R) (*14*). The regular secondary structures derived from the Ramachandran plot are represented by the color of the ribbon in green and red for β-turn and α-helix, respectively. The region from residue 11 to 15 has α-helix because of the CSH motif. (b) Peptide surface plot of the structure in panel a. The Tyr 13 aromatic ring is buried in the peptide folding, which in the hydrophobic core consists of Val 12, Tyr 13, Phe 14, Leu 17, Ile 19, and Ile 20. (c) Reverse side of the surface of the structure in panel b. (d) Crystal structure with the α-carbon ribbon (PDB entry 1EDN) (*6*). The irregular helix from residue 11 to 15 is likely caused by the structural bias of the intermolecular hydrogen bond between Tyr 13 of one molecule and Asp 8 of the other. The two residues are out of range of the regular structure in the Ramachandran plot. (e) Peptide surface plot of the structure in panel d. The Tyr 13 aromatic ring is exposed in the surface, and there is a hydrophobic surface in the crystalline dimerization interface. (f) Reverse side of the surface of the structure in panel e.

a hydrophobic core around the Tyr 13 side chain (Figure 1a,b). This is not consistent with the crystal structure (Figure 1d,e) but in good agreement with parameters obtained in NMR experiments as *J* coupling and sequential NOEs (*10*, *14*). Here, the hydrophobic core, which is usually found in globular proteins, is confirmed by another NMR technique, photochemically induced dynamic nuclear polarization (photo-CIDNP), accompanied by matrix-assisted laser desorption ionization time-of-flight mass spectrometry (MALDI-TOF-MS). We present here a new reference ET-1 structure and C-terminal folding, which should shed new light on ET receptor antagonist drug design.

MATERIALS AND METHODS

Photo-CIDNP NMR Experiments. All photo-CIDNP NMR measurements were carried out on a Bruker AMX 600 MHz spectrometer with irradiation by an argon ion laser (NEC-GLG3460) at a wavelength of 488 nm. ET-1 and endothelin-3 (ET-3) were purchased from Peptide Institute Inc. (Osaka, Japan). ET-1 C-terminal residues 11−21 [ET-1(11−21)] was synthesized by a solid-phase procedure on an Applied Biosystems model 431A automated peptide synthesizer on 0.5 mmol of Boc-Trp(CHO)-phenylacetoamidomethyl resin, and was elongated by Boc-amino acid HOBt esters with *N*,*N*′-dicyclohexylcarbodiimide. The peptides were dissolved in H_2O with D_2O (9:1, v/v), at 297.7 K, with 0.1 mM lumiflavin (luF), and were subjected to the experiments. The pH was adjusted with DCl and NaOD. The laser irradiation time before every acquisition (16 scans) was 500 ms. The photo-CIDNP signals have positive peak enhancement (for tryptophan aromatic ring protons) and negative peak enhancement (for tyrosine ring protons of the C_ϵ position). The photoexcited luF reacts reversibly with the residues to generate a luF−ET-1 radical pair. The back reaction of the radical pair yields nuclear spin polarization. However, the radical reaction is not completely reversible, as mentioned later, resulting in a decrease in the NMR signal intensities. Thus, 16 scans is a limitation of the irradiation for obtaining a good signal-to-noise ratio.

The ET samples suffered from 64 scans of CIDNP measurements (i.e., irradiation for a total of 32 s), which had a remarkable loss of the CIDNP signals, and were subjected to the MALDI-TOF MS experiment to check the molecular weight of the byproducts of the photoinduced radical reaction.

MALDI-TOF MS Experiments. MALDI-TOF MS spectra were measured on a LDI1700-MALDI-TOF MS system (Linear Scientific Inc.), with a −4.8 kV detector and a 3.9 mV/b digitizer. The matrix was sinapic acid. Laser energies were 2.34, 2.65, and 14.53 μJ for ET-1 without luF, ET-1 after laser irradiation with luF, and ET-3 after laser irradiation with luF, respectively. All preliminary laser irradiations were carried out under the same condition with photo-CIDNP experiments with a sample concentration of 0.16 mM.

NOESY Experiments. All NOESY measurements were carried out on a Bruker AMX 600 MHz spectrometer. ET-1 and ET-3 were dissolved in H_2O with D_2O (9:1, v/v), with 5% deuterated acetic acid, at 297.7 K and pH 3.0. The mixing time of NOESY runs was 350 ms.

RESULTS

At first, we performed photo-CIDNP NMR experiments to investigate the hydrophobic core around Tyr 13. The photo-CIDNP is a difference spectroscopic method that enhances the NMR signals of specific aromatic amino acid residues (tyrosine, tryptophan, and histidine) using a lumiflavin for the conformational probe (*21*). Since the lumiflavin can only interact with residues that are exposed to solvent, this technique can examine the folding of peptides. If ET-1 really has the hydrophobic core (Figure 1a,b), the photo-CIDNP signal intensities of Tyr 13 can be significantly reduced. Conversely, in the crystal structure, the Tyr 13 side chain is involved in intermolecular hydrogen bonds (*6*) (Figure 1d,e). If ET-1 has a monomeric form and the same

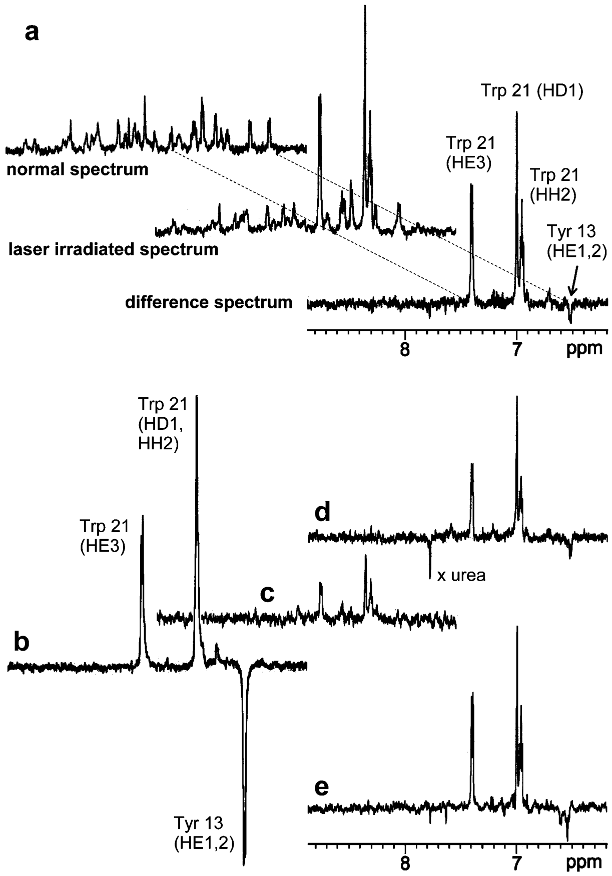

FIGURE 2: Photo-CIDNP spectra. (a) ET-1 at 0.16 mM at pH 3.0. The normal spectrum without the irradiation was subtracted from the laser-irradiated spectrum, resulting in the difference spectrum. (b) C-Terminal fragment of ET-1(11−21) at a concentration of 0.64 mM at pH 7.5. (c) ET-1 at a concentration of 0.64 mM at pH 3.0. (d) ET-1 at a concentration of 0.64 mM at pH 3.0 with 5 M urea. (e) ET-3 at a concentration of 0.16 mM at pH 3.0. All other experimental conditions are the same for all spectra. Only the difference spectra are displayed (b−e).

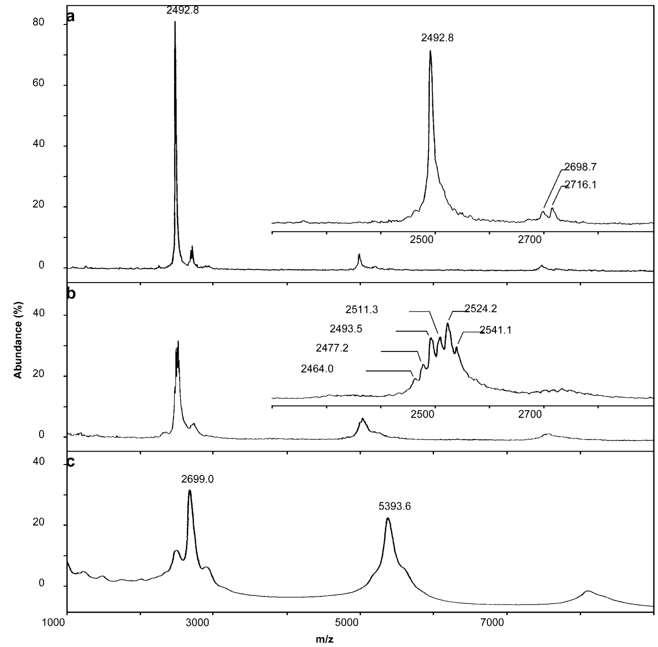

FIGURE 3: MALDI-TOF MS spectra of ET-1 and ET-3. (a) Intact ET-1 without lumiflavin. The calculated molecular weight of ET-1 is 2492, which is well matched with the main peak of $[M + H]^+$ (m/z 2492.8). Small peaks beside the main peak are caused by ionization matrix-bound peptides, sinapic acid (MW 224). (b) ET-1 after the photo-CIDNP experiment shown in Figure 2. (c) ET-3 after the photo-CIDNP experiment shown in Figure 2e. The calculated average molecular weight of intact ET-3 is 2643.

structure as the crystal under physiological conditions, we will observe a strong Tyr 13 photo-CIDNP signal.

Figure 2 shows photo-CIDNP spectra of ET-1 at a concentration of 0.16 mM. Despite clear Trp 21 signals enhanced by the irradiation, Tyr 13 CIDNP signal enhancements are very weak, as we expected. The Trp 21 signal enhancements agree with the solvent accessibility of the C-terminus (Figure 1a). Figure 2b shows a control experiment of C-terminal fragment ET-1(11−21), indicating clear photo-CIDNP signals for both tyrosine and tryptophan, which correspond to residues 13 and 21 in the ET-1 sequence, respectively. Because the fragment was not soluble at a lower pH, it was measured at pH 7.5, whereas ET-1 was not soluble at pH >4. However, there is no pH dependency for the free state of tyrosine CIDNP signals in this pH range, and thus, the strong suppression of Tyr 13 CIDNP signals in ET-1 indicates solvent inaccessibility for the side chain.

The ET-1 CIDNP signals were considerably attenuated at a higher concentration (0.64 mM) as shown in Figure 2c, and were recovered by adding urea (Figure 2d). This suggests that the existence of reversible peptide association originated in intermolecular hydrogen bonds. However, the apparent molecular weight determined by sedimentation analysis (MW 2500) indicates that the large majority of ET-1 molecules are in a monomer state at concentrations of <5 mM (*7*). The NMR peak line shapes (see Figure 4a) also support the monomeric form of ET-1 up to 2.5 mM. Thus, the amount of peptide in the association could be too small to be detected by the sedimentation analysis and one-dimensional (1D) NMR under the solution conditions. With a much higher concentration, the association by a hydrogen bond might be observable as in the ET-1 crystal structure. On the other hand, at 0.16 mM ET-1, adding urea (up to 6 M) has no impact on the CIDNP spectra or 1D NMR spectra, which resulted in the same spectra as Figure 2. Therefore, the solvent inaccessibility of the Tyr 13 side chain can be caused by the hydrophobic core, not the hydrogen bond.

Next, to distinguish an intramolecular hydrophobic core from the intermolecular interactions, we combined the measurements with MALDI-TOF MS for the preliminary laser-irradiated ET-1/lumiflavin solution. The photo-CIDNP radical reaction is not completely reversible and produces a significant amount of byproduct molecules. In the case of an associated molecule, the irreversible radical reaction can cause covalently bound peptides as byproducts, because of the rapid reaction compared with the molecular dissociation constant of the peptides. The results shown in Figure 3 demonstrate that the byproducts of ET-1 attacked by excited lumiflavin mainly originated from the monomer state (Figure 3b). The associated MS signals are just within the artifact level, e.g., ionization matrix-bound peptides. Therefore, it is confirmed that in ET-1 Tyr 13 is concealed by the intramolecular hydrophobic core around the residue as indicated by the three-dimensional structure.

The same experiments were performed for ET-3, another isoform of the endothelin family, which has the same C-terminal residues as ET-1 and receptor selectivity clearly

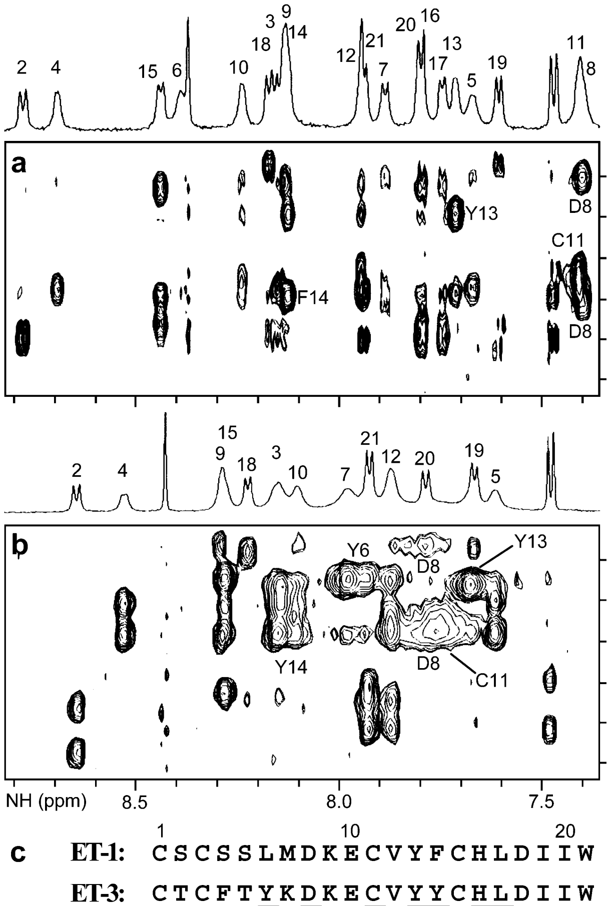

FIGURE 4: 1D and NOESY NMR spectra of ET-1 and ET-3 demonstrating a region of NH−$C_\beta H_2$ cross-peaks of AMX spin systems (Cys, Asp, Tyr, Phe, His, and Trp). Thr and Ser also have intraresidual cross-peaks in this region. (a) ET-1 concentration of 2.5 mM. The main chain amide proton assignments are indicated by sequence numbers on the 1D spectrum. Asp 8, Cys 11, Tyr 13, and Phe 14 intraresidual cross-peaks are labeled on the NOESY spectrum with their one-letter code. (b) ET-3 concentration of 2.5 mM. Tyr 6, Cys 11, Tyr 13, and Tyr 14 intraresidual cross-peaks are labeled with their one-letter code. The line broadening is caused by chemical exchange in the self-association equilibrium, and the broadening degrees reflect chemical shift differences in the exchange. (c) The amino acid sequences of ET-1 and ET-3 are given in the one-letter code. The residues of those that have strong line broadening in panel b are underlined.

different from that of ET-1 (*22*, *23*). The photo-CIDNP experiment with ET-3 resulted in spectra that are almost the same as those of ET-1 (Figure 2e). A monomeric form of the intact ET-3 was confirmed by sedimentation analysis [MW 2620 (with less than 5% error)] as well as MALDI-TOF MS ($[M + H]^+$, *m*/*z* 2642.0). However, the photoinduced radical-reacted ET-3 (after the CIDNP experiment) shows surprisingly different results (Figure 3c), indicating that ET-3 has an associated form under this condition. Almost half of the MS signal abundance has the dimer molecular weight. Because the association cannot be observed by sedimentation analysis and MS, the association can be reversible in fast equilibrium, likely caused by weak molecular interaction such as hydrophobic interaction. As far as we know, this is the first study using the photoinduced radical reaction with MALDI-TOF MS to analyze peptide association.

The self-association equilibrium of ET-3 is also observed by 1D and two-dimensional (2D) NMR spectra. Figure 4 shows differences of the NMR line shapes between ET-1 and ET-3 under the same solution conditions, demonstrating NH−$C_\beta H_2$ cross-peaks of AMX spin systems (*24*). Despite the uniform line width of the ET-1 spectrum just modulated by *J* couplings (Figure 4a), ET-3 cross-peaks indicate significant sequence specific line broadening at a concentration of 2.5 mM (Figure 4b). ET-3 has three tyrosines in its sequence (Tyr 6, Tyr 13, and Tyr 14), and ET-1 has only one, Tyr 13 (Figure 4c). The three tyrosines of ET-3 are uniformly concealed in solution as indicated by the photo-CIDNP experiments (Figure 2e), and have broadened cross-peaks (Figure 4b). This indicates that ET-3 exists in the self-association equilibrium in the concentration range of 0.16−2.5 mM, as detected by MALDI-TOF MS experiments, and the three tyrosines are responsible for the intermolecular interaction. It is noteworthy that C-terminal residues Ile 19, Ile 20, and Trp 21 have a very small influence on the equilibrium (Figure 4b). The residues, which are responsible for the activity, could not participate in ET-3 self-association.

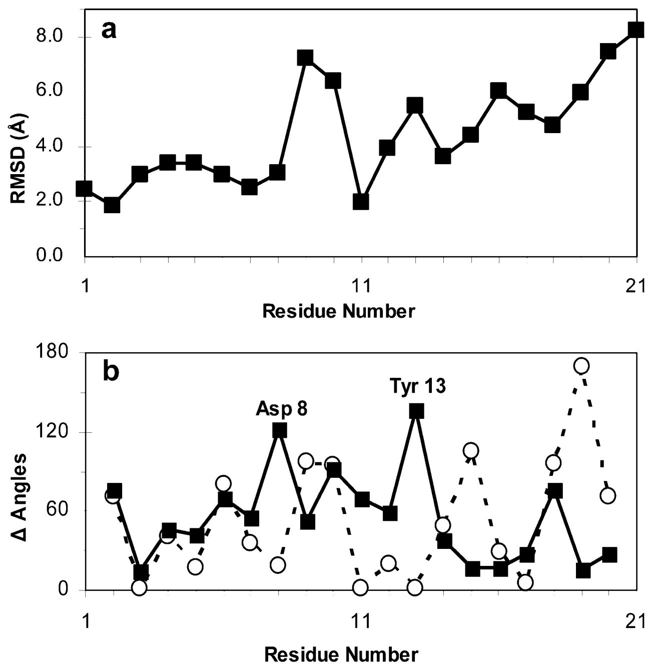

FIGURE 5: Structural comparison between solution (*14*) and crystalline (*6*) ET-1. (a) Averaged backbone rmsd values of the NMR structures overlaying all residues (1−21) on the crystal structure are elucidated for all residues and plotted against them. (b) Backbone dihedral angle difference between the solution (minimum energy structure) and crystalline ET-1. Absolute values of the differences are plotted against residue number for ϕ (■) and ψ (○) angles. The remarkably large differences for ϕ angles of Asp 8 and Tyr 13 are due to the intermolecular hydrogen bond between residues of one molecule and the other in the crystalline dimer.

DISCUSSION

Now it is clear that ET-1 has an intramolecular hydrophobic core under physiological conditions, and has a different folding in the crystalline form. The structural comparison between the solution and crystalline ET-1 shows a large root-mean-square deviation (rmsd) value for backbone atoms overlaid for all residues, i.e., 4.4 Å. The large rmsd value is caused by structural differences of residues from 9 to 21 (Figure 5a). The N-terminal region of residues 1−8 overlaid for this region is similar for the two structures (rmsd

= 1.5 Å). It is clear that an intermolecular hydrogen bond between Tyr 13 OH and Asp 8 carbonyl oxygen in the crystal structure (*6*) causes the large difference (Figure 5b), and strongly influences the C-terminal folding, which originates from Tyr 13.

In the report of the crystal structure (*6*), the authors discussed that the intermolecular hydrogen bond can be ignored, because it is not in the C-terminal region. They also mentioned that residues 8 and 13 are in the N-terminal region and have a folding similar to those of previously published NMR structures. In fact, the region from residue 1 to 15 has a relatively small rmsd (2.0 Å) in the two structures, because of the two disulfide bonds (CSH motif), which does not support their discussion. Moreover, any of the intermolecular interactions should not be ignored in such a small peptide. The energy term of the hydrogen bond is much larger than that of a hydrophobic interaction, and is very decisive for the peptide folding.

In the solution structure we have reported (*14*), the peptide surface of Tyr 13 is surrounded by hydrophilic residues Lys 9, Glu 10, and Asp 18, and the Trp 21 ring is close to the positive and negative charge, as well as the Phe 14 ring (Figure 1b,c). The structure can sufficiently be matched to the many antagonist molecules, and can explain broad structural findings (*12*, *13*, *25*, *26*). The ring formation and charge location agree well with the antagonist structures. In the crystal structure, the residues are localized on the edge of the dimerization hydrophobic interface (Figure 1e,f). We believe that the solution structure derived from NMR as well as the structural features of ET-1 and ET-3 will provide a new horizon for the ET receptor antagonist design.

ACKNOWLEDGMENT

We thank Ms. Susan C. DiClemente, Dr. Norio Mimura, and Dr. Takanori Kanazawa for their helpful discussion and Dr. Robert Hof, Dr. Manuel Peitsch, Mr. Hideaki Numa, and Dr. Atsuko Nosaka for their support.

REFERENCES

1. Yanagisawa, M., Kurihara, H. K. S., Tomobe, Y., Kobayashi, M., Mitsui, Y., Yazaki, Y., Goto, K., and Masaki, T. (1988) A novel potent vasoconstrictor peptide produced by vascular endothelial cells, *Nature 332*, 411−415.
2. Sakai, S., Miyauchi, T., Kobayashi, M., Yamaguchi, I., Goto, K., and Sugishita, Y. (1996) Inhibition of myocardial endothelin pathway improves long-term survival in heart failure, *Nature 384*, 353−355.
3. Schiffrin, E. L. (2000) Endothelin: role in experimental hypertension, *J. Cardiovasc. Pharmacol. 35* (Suppl. 2), S33−S35.
4. Spinella, F., Rosano, L., Di Castro, V., Natali, P. G., and Bagnato, A. (2002) Endothelin-1 induces vascular endothelial growth factor by increasing hypoxia-inducible factor-1a in ovarian carcinoma cells, *J. Biol. Chem. 277*, 27850−27855.
5. Nelson, J., Bagnato, A., Battistini, B., and Nisen, P. (2003) The endothelin axis: emerging role in cancer, *Nat. Rev. Cancer 3*, 110−116.
6. Janes, R. W., Peapus, D. H., and Wallace, B. A. (1994) The crystal structure of human endothelin, *Nat. Struct. Biol. 1*, 311−319.
7. Tamaoki, H., Kobayashi, Y., Nishimura, S., Ohkubo, T., Kyogoku, Y., Nakajima, K., Kumagaye, S., Kimura, T., and Sakakibara, S. (1991) Solution conformation of endothelin determined by means of ^{1}H NMR spectroscopy and distance geometry calculations, *Protein Eng. 4*, 509−518.
8. Krystek, S. R., Jr., Bassolino, D. A., Novotny, J., Chen, C., Marschner, T. M., and Andersen, N. H. (1991) Conformation of endothelin in aqueous ethylene glycol determined by ^{1}H-NMR and molecular dynamics simulations, *FEBS Lett. 281*, 212−218.
9. Saudek, V., Hoflack, J., and Pelton, J. T. (1991) Solution conformation of endothelin-1 by proton NMR, *Int. J. Pept. Protein Res. 37*, 174−179.
10. Wallace, B. A., Janes, R. W., Bassolino, D. A., and Krystek, S. R., Jr. (1995) A comparison of X-ray and NMR structures for human endothelin-1, *Protein Sci. 4*, 75−83.
11. Nakajima, K., Kubo, S., Kumagaye, S., Nishio, H., Kuroda, H., Tsunemi, M., Inui, T., Kuroda, H., Chino, N., Watanabe, T. X., Kimura, T., and Sakakibara, S. (1989) Synthesis of endothelin-1 analogs, endothelin-3, and sarafotoxin S6b: structure−activity relationships, *J. Cardiovasc. Pharmacol. 13* (Suppl. 5), S8−S12.
12. Remuzzi, G., Perico, N., and Benigni, A. (2002) New therapeutics that antagonize endothelin: promises and frustrations, *Nat. Rev. Drug Discovery 1*, 986−1001.
13. Funk, O. F., Kettmann, V., Drimal, J., and Langer, T. (2004) Chemical function based pharmacophore generation of endothelin-A selective receptor antagonists, *J. Med. Chem. 47*, 2750−2760.
14. Takashima, H., Mimura, N., Ohkubo, T., Yoshida, T., Tamaoki, H., and Kobayashi, Y. (2004) Distributed computing and NMR constraint-based high-resolution structure determination: applied for bioactive peptide endothelin-1 to determine C-terminal folding, *J. Am. Chem. Soc. 126*, 4504−4505.
15. Snow, C. D., Nguyen, H., Pande, V. S., and Gruebele, M. (2002) Absolute comparison of simulated and experimental protein-folding dynamics, *Nature 420*, 102−106.
16. Bontems, F., Roumestand, C., Gilquin, B., Menez, A., and Toma, F. (1991) Refined structure of charybdotoxin: common motifs in scorpion toxins and insect defensins, *Science 254*, 1521−1523.
17. Kobayashi, Y., Sato, A., Takashima, H., Tamaoki, H., Nishimura, S., Kyogoku, Y., Ikenaka, K., Kondo, T., Mikoshiba, K., Hojo, H., Aimoto, S., and Moroder, L. (1991) A new α-helical motif in membrane active peptides, *Neurochem. Int. 18*, 525−534.
18. Kobayashi, Y., Takashima, H., Tamaoki, H., Kyogoku, Y., Lambert, P., Kuroda, H., Chino, N., Watanabe, T. X., Kimura, T., Sakakibara, S., and Moroder, L. (1991) The cystine-stabilized α-helix: a common structural motif of ion-channel blocking neurotoxic peptides, *Biopolymers 31*, 1213−1220.
19. Lapthom, A. J., Janes, R. W., Isaacs, N. W., and Wallace, B. A. (1995) Cystine nooses and protein specificity, *Nat. Struct. Biol. 2*, 266−268.
20. Tamaoki, H., Miura, R., Kusunoki, M., Kyogoku, Y., Kobayashi, Y., and Moroder, L. (1998) Folding motifs induced and stabilized by distinct cystine frameworks, *Protein Eng. 11*, 649−659.
21. Kaptein, R., Dijkstra, K., and Nicolay, K. (1978) Laser photo-CIDNP as a surface probe for proteins in solution, *Nature 274*, 293−294.
22. Arai, H., Hori, S., Aramori, I., Ohkubo, H., and Nakanishi, S. (1990) Cloning and expression of a cDNA encoding an endothelin receptor, *Nature 348*, 730−732.
23. Sakurai, T., Yanagisawa, M., Takuwa, Y., Miyazaki, H., Kimura, S., Goto, K., and Masaki, T. (1990) Cloning of a cDNA encoding a non-isopeptide-selective subtype of the endothelin receptor, *Nature 348*, 732−735.
24. Wuthrich, K. (1986) *NMR of proteins and nucleic acids*, John Wiley & Sons, New York.
25. Aumelas, A., Kubo, S., Chino, N., Chiche, L., Forest, E., Roumestand, C., and Kobayashi, Y. (1998) Formation of native disulfide bonds in endothelin-1. Structural evidence for the involvement of a highly specific salt bridge between the prosequence and the endothelin-1 sequence, *Biochemistry 37*, 5220−5230.
26. Laricchia-Robbio, L., and Revoltella, R. P. (2004) Comparison between the surface plasmon resonance (SPR) and the quartz crystal microbalance (QCM) method in a structural analysis of human endothelin-1, *Biosens. Bioelectron. 19*, 1753−1758.

BI048649U